

Structural Properties of Graphene and Carbon Nanotubes

Brian Shevitski

Department of Physics and Astronomy, University of California Los Angeles, Los Angeles, CA 90095

(Dated: September 28, 2010)

Various structural properties of graphitic materials are investigated in a transmission electron microscope. Using electron diffraction the hexagonal lattice and bond length of graphene are verified. Also multiple views of multiwalled carbon nanotubes are used to create a tomographic reconstruction.

I. INTRODUCTION

Graphene was discovered in 2004 and has since sparked much interest in the field of condensed matter physics. Graphene is an atomically thin sheet of carbon arranged in a two dimensional honeycomb crystal. The Mermin-Wagner Theorem predicts that a perfect crystal can not exist in two dimensional space, so it was surprising when graphene was first observed[1]. The existence of graphene has since been explained by the idea that graphene has an intrinsic roughness. This rippling makes graphene a nearly perfect two dimensional crystal in three dimensional space[2, 3], which is not forbidden.

Graphene has been called the “mother of all graphitic forms”[4] because it can be wrapped into buckyballs, rolled into carbon nanotubes and stacked into graphite. High resolution images of a sheet of graphene and a multiwalled carbon nanotube are shown in Fig. 1 and Fig. 2. These materials are not only important new testing grounds for fundamental physics such as relativistic quantum mechanics and low dimensional thermodynamics, but also have potential applications to nanoscale technology such as high speed transistors and lasers.

We can not investigate the structural properties of these graphitic materials using conventional optical microscopes because it is not possible to resolve anything smaller than a wavelength of the light used to illuminate the sample. Light in the visible spectrum has a wavelength $\lambda \approx 500$ nm. Due to the sub-nanometer length scales of the structures of graphene and carbon nanotubes it is necessary to use an electron microscope to investigate their structural properties. We operate using electrons at 80 kV because graphene and carbon nanotubes are unstable under higher energy electron beams and samples are rapidly destroyed[5, 6]. An electron with this energy is traveling at almost one half the speed of light and we must take relativistic effects into account. The relativistic wavelength of an electron is,

$$\lambda = \frac{h}{mc\sqrt{\left(1 + \frac{eV}{E_0}\right)^2 - 1}}, \quad (1)$$

where h is the Planck constant, m is the electron rest mass, c is the speed of light, e is the magnitude of the electron charge, V is the voltage the electron is accelerated through and E_0 is the electron rest energy. An 80 keV electron has a wavelength of ~ 4.18 pm which allows

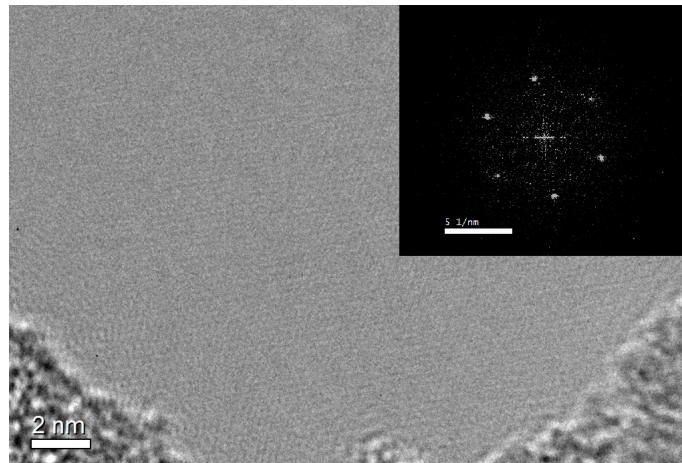


FIG. 1: High resolution TEM image of a suspended sheet of graphene. The Fourier transform of the image is shown in the top right. The darker portions are remnants of the SiO_2 and Si_3N_4 membrane that were not removed by the HF etch.

us to resolve much smaller structures than we can using light in the visible spectrum. The main factor limiting resolution in the electron microscope is spherical aberration which arises due to the inability to make perfect lenses to focus the electron beam to a point. The smallest object that can be resolved is given approximately by

$$\delta \cong (C_s \lambda^3)^{\frac{1}{4}}, \quad (2)$$

where C_s is the spherical aberration of the microscope and λ is the wavelength of the electrons[7]. For our microscope, an FEI Titan 80-300, $C_s \approx 1.2$ mm and $\delta \cong .35$ nm.

II. CRYSTAL THEORY

An ideal crystal is formed by an infinite repetition of identical groups of atoms. Each group of atoms, called the basis, is attached to a point on a periodic array called the lattice. In the case of ideal graphene, a two atom basis is attached to a hexagonal lattice and the result is a two dimensional honeycomb crystal as shown in Fig. 3. Any point on the crystal lattice can be represented as a vector,

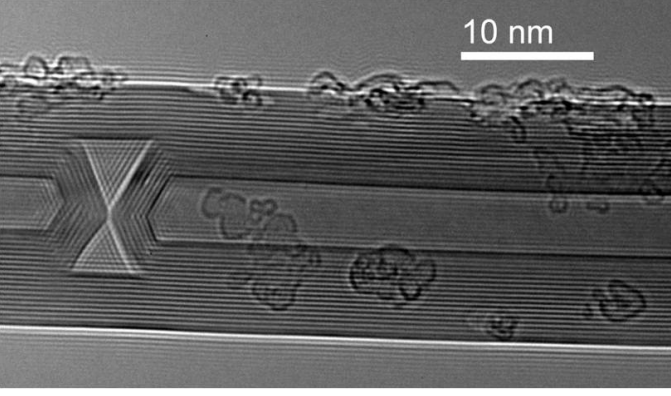


FIG. 2: High resolution TEM image of a multiwall carbon nanotube. Nanotube wall spacing is 0.34 nm. The hourglass shape on the left is called a bamboo defect and the amorphous material in the image is nanotube debris. At 80 kV it is possible to resolve the walls and core of the nanotube but it is not possible to resolve positions of atoms. At higher energies atomic resolution is possible but nanotubes are unstable.

$$\mathbf{R} = n_1 \mathbf{a}_1 + n_2 \mathbf{a}_2, \quad (3)$$

where n_1 and n_2 are integers and \mathbf{a}_1 and \mathbf{a}_2 are known as the primitive vectors of the crystal. A unit cell and primitive vectors are shown for graphene in Fig. 4.

We must also construct the reciprocal lattice of graphene in order to interpret its diffraction pattern. Each primitive vector of the reciprocal lattice is orthogonal to two primitive vectors of the crystal lattice. The reciprocal lattice vectors \mathbf{b}_1 , \mathbf{b}_2 and \mathbf{b}_3 have the property,

$$\mathbf{b}_i \cdot \mathbf{a}_j = 2\pi \delta_{ij}, \quad (4)$$

where $\delta_{ij} = 1$ if $i = j$ and $\delta_{ij} = 0$ if $i \neq j$. The construction of the reciprocal lattice vectors follow from (4),

$$\mathbf{b}_1 = 2\pi \frac{\mathbf{a}_2 \times \mathbf{a}_3}{\mathbf{a}_1 \cdot \mathbf{a}_2 \times \mathbf{a}_3}, \quad (5)$$

$$\mathbf{b}_2 = 2\pi \frac{\mathbf{a}_3 \times \mathbf{a}_1}{\mathbf{a}_1 \cdot \mathbf{a}_2 \times \mathbf{a}_3}, \quad (6)$$

$$\mathbf{b}_3 = 2\pi \frac{\mathbf{a}_1 \times \mathbf{a}_2}{\mathbf{a}_1 \cdot \mathbf{a}_2 \times \mathbf{a}_3}, \quad (7)$$

where \mathbf{a}_1 and \mathbf{a}_2 are the primitive vectors of the crystal and \mathbf{a}_3 is the \hat{z} unit vector. Any point on graphene's reciprocal lattice can be represented as a vector

$$\mathbf{G} = m_1 \mathbf{b}_1 + m_2 \mathbf{b}_2, \quad (8)$$

Where m_1 and m_2 are integers. The reciprocal lattice of graphene and its primitive vectors are shown in Fig. 5.

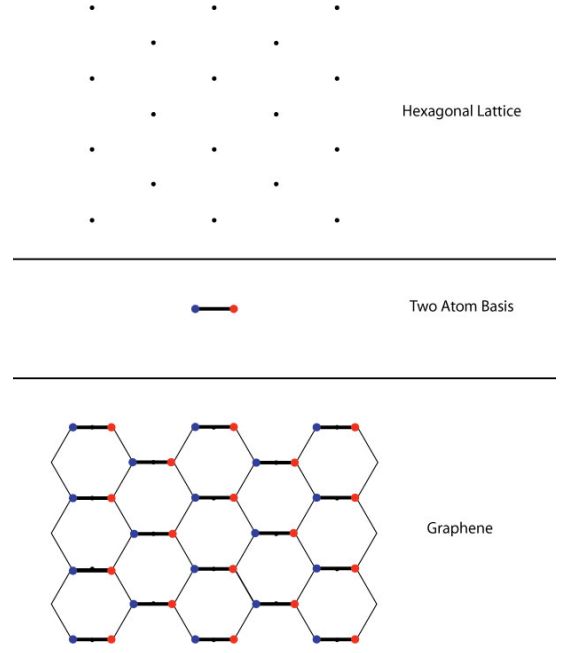


FIG. 3: A 2D honeycomb crystal is formed by placing a two atom basis to each point on a hexagonal lattice.

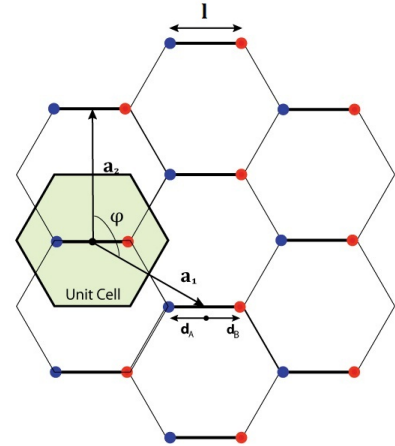


FIG. 4: Graphene consists of a two atom basis superimposed onto a hexagonal lattice. Each unit cell contains one lattice point and a two atom basis. Any lattice point can be reached by adding an integral number of primitive vectors. The vectors \mathbf{d}_A and \mathbf{d}_B point from a lattice point to an atom in the basis and are used in calculating the structure factor. $|\mathbf{a}_1| = |\mathbf{a}_2| = \sqrt{3}l$, $|\mathbf{d}_A| = |\mathbf{d}_B| = \frac{l}{2}$, $\phi = 120^\circ$

The analog of adding a basis to a crystal lattice is adding a structure factor to a reciprocal lattice. A lattice and a basis determine a crystal whereas a structure factor, denoted S_G , and a reciprocal lattice describe a diffraction pattern. This will be discussed further in sec. IV

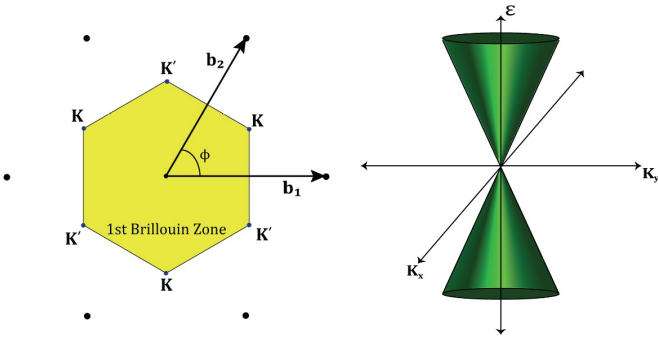


FIG. 5: Primitive vectors of graphene's reciprocal lattice. The 1st Brillouin zone is a unit cell of the reciprocal lattice. Near the points k and k' the energy of the electrons in graphene depend linearly on their wavenumber. This is similar to the behavior of a relativistic particle whose behavior is described by the Dirac equation. $|b_1| = |b_2| = \frac{4\pi}{3l}$, $\phi = 60^\circ$

III. DIFFRACTION THEORY

One way to confirm the geometry of the crystal lattice of graphene is to take diffraction images of a sample. In our microscope diffraction is needed because the resolution at 80 kV is not sufficient to image atomic positions. Consider a beam of electrons of wave vector \mathbf{k} elastically scattered from a sample. The scattered electrons will have a new wave vector \mathbf{k}' with the same magnitude as \mathbf{k} . Fourier analysis shows that the set of reciprocal lattice vectors \mathbf{G} determines the possible scattering vectors $\Delta\mathbf{k} = \mathbf{k}' - \mathbf{k}$ [9, 10]. The Bragg condition for diffraction is given by the equation,

$$\mathbf{G} = \Delta\mathbf{k}. \quad (9)$$

From (9) and Fig. (6) using geometric arguments and the small angle approximation we find that

$$G = k\theta = \frac{2\pi\theta}{\lambda}. \quad (10)$$

We can use this condition to relate the position of the observed intensity peaks where elastically scattered electrons constructively interfere to the set of reciprocal lattice vectors \mathbf{G} . This allows us to determine the C-C bond length in real space by measuring the position of the diffraction peaks in reciprocal space.

IV. DIFFRACTION ANALYSIS

In order to analyze the diffraction pattern of graphene we first need to break the primitive vectors into components. The primitive vectors of graphene are

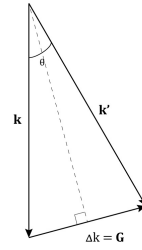


FIG. 6: The Bragg condition for diffraction for an incident beam of wave vector \mathbf{k} elastically scattered through an angle θ and the resultant wave vector \mathbf{k}' gives the allowed diffraction peaks.

$$\mathbf{a}_1 = \frac{3l}{2} \left(\hat{\mathbf{x}} - \frac{\sqrt{3}}{3} \hat{\mathbf{y}} \right), \quad (11)$$

$$\mathbf{a}_2 = \sqrt{3}l\hat{\mathbf{y}}, \quad (12)$$

$$\mathbf{a}_3 = \hat{\mathbf{z}}, \quad (13)$$

where l is the C-C bond length. Next using (5), (6) and (7) we find the primitive reciprocal lattice vectors which are

$$\mathbf{b}_1 = \frac{4\pi}{3l} \hat{\mathbf{x}} \quad (14)$$

$$\mathbf{b}_2 = \frac{4\pi}{3l} \left(\frac{1}{2} \hat{\mathbf{x}} + \frac{\sqrt{3}}{2} \hat{\mathbf{y}} \right) \quad (15)$$

$$\mathbf{b}_3 = 2\pi\hat{\mathbf{z}} \quad (16)$$

To verify the bond length we measure the distance from the center of the pattern to the intensity peak. The distance measured in reciprocal space is defined as

$$q \equiv \frac{\theta}{\lambda} \quad (17)$$

We then substitute this into (10), find the magnitude of G from (8) and simplify for the following equation that relates measurements made on the diffraction pattern to the bond length

$$q = \frac{2}{3l} \sqrt{m_1^2 + m_1 m_2 + m_2^2} \quad (18)$$

We count the number of \mathbf{b}_1 and \mathbf{b}_2 vectors that comprise each \mathbf{G} and index the diffraction pattern (Fig. 9) for

easy identification of m_1 and m_2 . We then measure q on the diffraction image and comparing the result to what is predicted by (18) using the currently accepted bond length of $l = .142$ nm[8]. This not only verifies the bond length but also confirms that our theory is sound.

The intensity of the diffraction peak depends on a quantity called the structure factor denoted by S_G . The structure factor is defined as

$$S_G = \sum_{basis} f_j \exp [i\mathbf{G} \cdot \mathbf{d}_j]. \quad (19)$$

where f_j is known as the atomic form factor of the j th atom of the basis.

$$\mathbf{d}_A = \frac{l}{2} \hat{\mathbf{x}} \quad (20)$$

$$\mathbf{d}_B = -\frac{l}{2} \hat{\mathbf{x}} \quad (21)$$

Because graphene has a two atom basis (19) becomes

$$S_G = f_A \exp [i\mathbf{G} \cdot \mathbf{d}_A] + f_B \exp [i\mathbf{G} \cdot \mathbf{d}_B]. \quad (22)$$

Graphene is composed entirely carbon so $f_A = f_B = f$. Also $\mathbf{d}_A = -\mathbf{d}_B = \mathbf{d}$.

$$S_G = 2f \frac{\exp [i\mathbf{G} \cdot \mathbf{d}] + \exp [-i\mathbf{G} \cdot \mathbf{d}]}{2} \quad (23)$$

Simplifying this gives

$$S_G = 2f \cos (\mathbf{G} \cdot \mathbf{d}). \quad (24)$$

Solving $\mathbf{G} \cdot \mathbf{d}$ from (14), (15) and (20) gives

$$S_G = 2f \cos \left[\frac{\pi}{3} (2n_1 + n_2) \right]. \quad (25)$$

The structure factor can only take values of, $\pm f$ and $\pm 2f$.

V. DIFFRACTION RESULTS

From the geometry of the observed diffraction pattern we can conclude that graphene does indeed have a hexagonal lattice. Also the measurements made on the diffraction pattern agree with theory to within one percent. Results of the diffraction analysis are summarized in Table I.

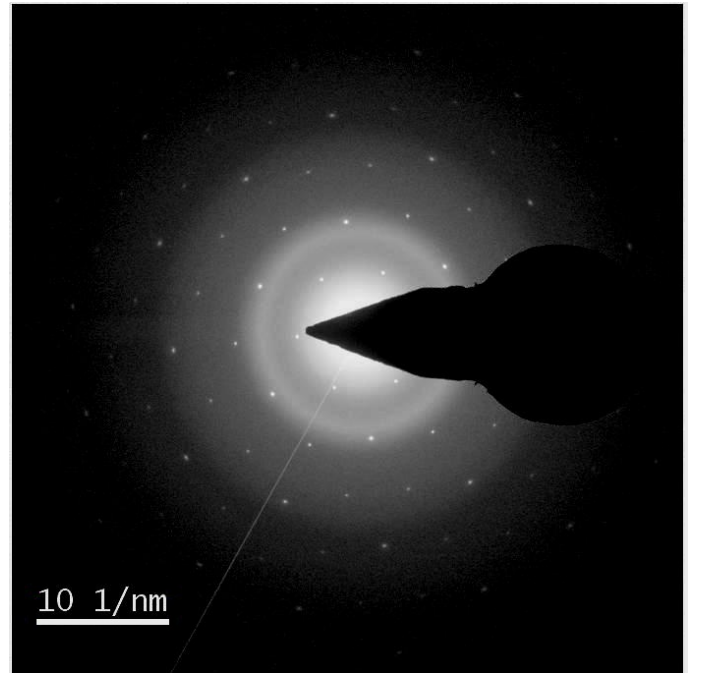


FIG. 7: The diffraction pattern of graphene is a hexagonal lattice. The large black shape in the middle is a beam blocker which protects the camera from being damaged. The small bright spots are diffraction peaks from the graphene. The large rings are caused by scattering from amorphous material that was not removed with the membrane of SiO_2 and Si_3N_4 the sample was originally deposited on. This image uses a log scale for intensity so more peaks can be easily seen

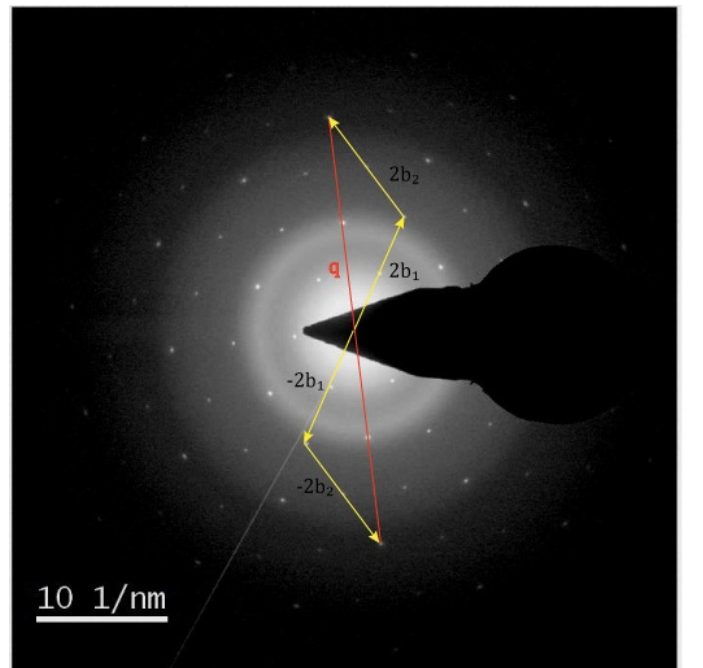


FIG. 8: The vector q connecting opposite peaks in the same order must be made by an integer number of reciprocal lattice primitive vectors.

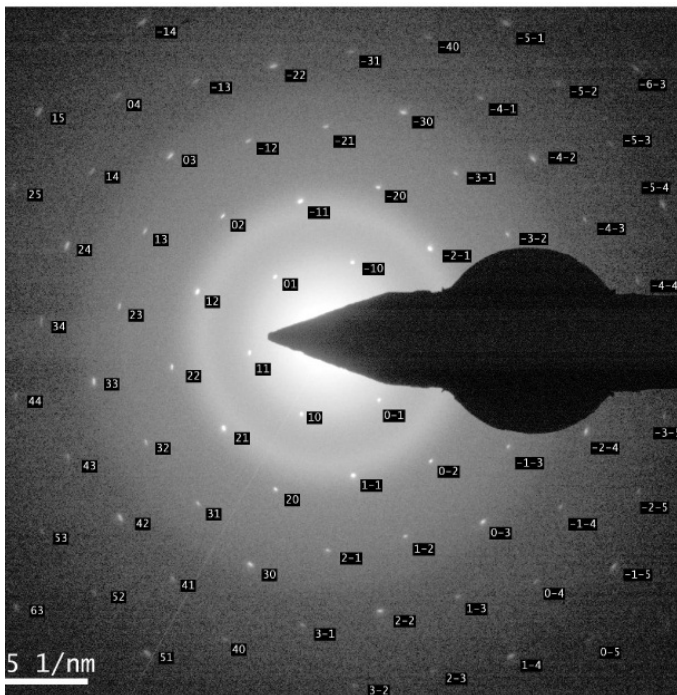


FIG. 9: The diffraction pattern is indexed for easier identification of m_1 and m_2 . The image is brightened and a log scale is used so more peaks can be easily identified

q_{raw} (1/nm)	q_{scaled} (1/nm)	m_1	m_2	$ M $	q_{theo} (1/nm)	S_G
$4.55 \pm .04$	$4.65 \pm .05$	1	0	1	4.69	f
$7.88 \pm .10$	$8.06 \pm .10$	1	1	1.73	8.13	$2f$
$9.11 \pm .09$	$9.32 \pm .10$	2	0	2	9.39	f
$12.09 \pm .11$	$12.36 \pm .12$	2	1	2.65	12.42	f
$13.78 \pm .16$	$14.09 \pm .13$	3	0	3	14.08	f
$15.96 \pm .15$	$16.31 \pm .17$	2	2	3.46	16.26	$2f$
$16.64 \pm .15$	$16.99 \pm .17$	3	1	3.61	16.93	f
$18.58 \pm .15$	$18.99 \pm .17$	0	4	4	18.78	$2f$

TABLE I: Sample of diffraction pattern analysis. $|M|$ denotes the value $\sqrt{m_1^2 + m_1 m_2 + m_2^2}$. The currently accepted bond length of $b = .142$ nm is used to calculate q_{theo} and is compared to the scaled measurement of the diffraction pattern q_{scaled} . q_{scaled} is computed by a statistical analysis of the points q_{raw} . All values of q_{scaled} are within two standard deviations of q_{theo} .

VI. ERROR ANALYSIS

The raw data needed to be corrected due to error caused by the image calibration. Using statistical analysis the data is scaled in order to correct for this [11]. The best data offset δ is found by minimizing the value of χ^2 as given by

$$\chi^2 = \sum_{i=1}^n \chi_i^2 = \sum_{i=1}^n \left(\frac{(q_{exp}\delta)_i - (q_{theo})_i}{\sigma_i} \right)^2. \quad (26)$$

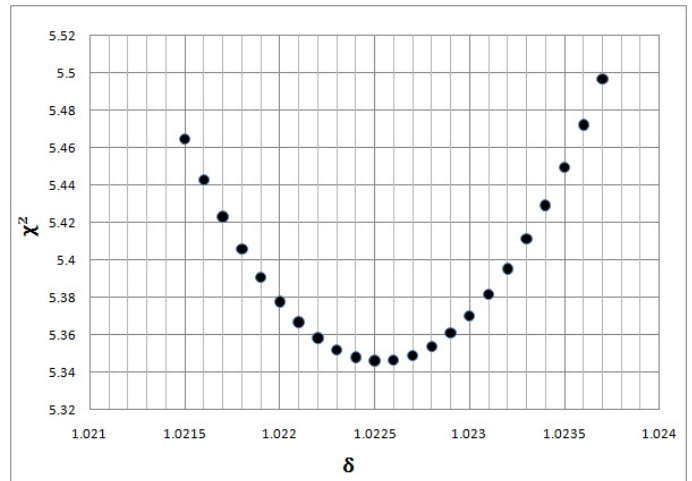


FIG. 10: In order to properly scale the data χ^2 was plotted for trial values of δ . The choice of δ that minimizes χ^2 is used to scale the raw data. For the data set presented $\delta = 1.022 \pm 0.004$.

where the summation is carried out over each data point and σ_i is the error of the associated data point.

VII. TOMOGRAPHY

Another method for examining the structure of graphene and carbon nanotubes is tomographic reconstruction. Tomography uses sectional views to reconstruct a 3D map of an object. This method allows one to create a map of an entire object as opposed to being limited to surface information using methods such as atomic force microscopy. Using electron tomography one can obtain a real 3D view of an object with nanometer-scale resolution. Electron tomography is typically used in the biomedical field in probing the structures of viruses and cells but has also been successfully applied to materials science. The tomography process consists of three main steps: acquiring a tilt series, aligning successive images, and reconstructing a volume.

A. Tilt Series

The raw data of a tomographic reconstruction consists of a series of TEM images taken at different angles called a tilt series. Each TEM image is a 2D projection of the sample. Tomography depends on the fact that the Fourier transform of a 2D projection of a 3D object is the same as the Fourier transform of the corresponding central slice of the 3D object [12]. Using this fact it is possible to build up the 3D Fourier transform of the object one plane at a time and take the inverse Fourier transform in order to reconstruct the original object.

B. Alignment

In order for the reconstruction to be accurate the tilt series must be properly aligned. The most common method of alignment first uses the cross-correlation algorithm to get a coarse alignment. The cross-correlation of two images is defined as

$$C(x, y) = F^{-1} [\mathcal{F} [I_1(x, y)] * \mathcal{F} [I_2(x, y)]] \quad (27)$$

where $\mathcal{F} [I_1(x, y)]$ and $\mathcal{F} [I_2(x, y)]$ are the Fourier transforms of the images to be aligned. F^{-1} denotes the inverse Fourier transform and $*$ denotes the convolution operation. The cross-correlation will have a sharp peak at the coordinate (x_0, y_0) where the two images have the best alignment. The location of this peak is then used to shift each image in order for the alignment to be optimized [13]. Also each image must be stretched by a factor of $\frac{1}{\cos \psi}$, where ψ is the tilt angle of the image, to correct for changes due to tilt geometry [14]. This process is carried out on each successive image in order to align the entire series. A fine alignment is then achieved by tracking small fiducial markers, usually gold, through the series. Alignment steps are carried out and reiterated until there is no noticeable change in successive image alignments.

C. Reconstruction

Once the tilt series is properly aligned the object is reconstructed plane by plane. Several algorithms are used, the most common being Weighted Back Projection (WBP) and Simultaneous Iterative Reconstruction Technique (SIRT) methods. These algorithms take the 3D Fourier transform of the object in reciprocal space and turn it into a reconstructed object in real space [15].

VIII. LIMITS OF TOMOGRAPHY

The resolution of a tomographic reconstruction is limited by three main factors assuming the image series is perfectly aligned: the number of views in the data, the object size, and the maximum angle the sample is tilted through [16].

The resolution in the direction parallel to the tilt axis d_x is the same as the resolution in the original projection image. The resolution in the directions perpendicular to the tilt axis of an object of diameter D , reconstructed using N views is given by

$$d_y = d_z = \frac{\pi D}{N} \quad (28)$$

However this assumes that the reconstruction uses views that go from $\pm 90^\circ$. In practice the maximum angle the sample is tilted through is not 90° due to restrictions

of the TEM. In this case the resolution in the direction parallel to the optical axis d_z of a sample tilted through a maximum angle of α experiences an elongation given by

$$e_z = \sqrt{\frac{2\alpha + \sin(2\alpha)}{2\alpha - \sin(2\alpha)}}, \quad (29)$$

and the resolution is

$$d_z = d_y e_z. \quad (30)$$

For the carbon nanotube reconstruction presented $D \approx 40$ nm, $N = 65$ and $\alpha = 58^\circ$. Assuming perfect alignment the resolution of the reconstruction is approximately

$$d_y \cong 1.9 \text{ nm} \quad (31)$$

$$e_z \cong 1.6 \quad (32)$$

$$d_z \cong 3.1 \text{ nm} \quad (33)$$

Due to the elongation factor, d_z is not good enough to resolve the walls of the nanotubes in this sample.

However it is possible to achieve atomic resolution using tomography. Using a different experimental setup in the TEM it is possible to tilt the sample through a maximum angle of $\alpha = 70^\circ$. If the object to be reconstructed is smaller such as a 2 nm gold particle it is entirely possible to resolve individual atoms. From (28) and (29) the minimum number of views needed to achieve atomic resolution of $d_z = a_0 = 0.134$ nm is 48.

In contrast, if one were trying to reconstruct a nanotube of diameter $D = 15$ nm with a maximum tilt angle $\alpha = 58^\circ$ it would be a daunting task to resolve the tube walls. This would require a resolution $d_z = 0.34$ nm which would in turn require using $N = 223$ views. This task is not currently feasible due to limitations of the TEM.

IX. CARBON NANOTUBE TOMOGRAPHY

A section of the carbon nanotube tilt series is shown in Fig. 11. In this image the two nanotubes are projected through one another and the vertical orientation of the tubes is unclear. After reconstruction the relative position of the tubes becomes apparent as illustrated in Fig. 12.

X. EXPERIMENTAL METHODS

Graphene samples were prepared using chemical vapor deposition (CVD) on a SiO_2 and Si_3N_4 membrane followed by an HF etch. Carbon nanotubes were prepared using arc discharge and were deposited on membrane and etched in the same manner as the graphene samples. 5 nm gold particles were deposited on the nanotubes to use as fiducial markers in aligning the image tilt series.

Diffraction images and carbon nanotube tilt series were acquired at UCLA by Matt Mecklenburg using a Titan 80-300 TEM at 80 kV. To verify the bond length the intensity maxima of opposite peaks in the same order were located in the diffraction pattern and the distance between them was measured. Diffraction pattern measurements were made using Digital Micrograph and ImageJ software. Tilt series were coarsely aligned using the cross-correlation method and finely aligned using gold bead tracking in the IMOD eTomo program. Volume was reconstructed using the SIRT method in Inspect3d. Volume was manipulated, filtered and imaged using Chimera and Amira software.

XI. CONCLUSION

From the diffraction pattern of the suspended graphene sheet the hexagonal lattice and bond length of graphene was verified. Preliminary reconstructions are promising and tomography has been verified as a useful method for investigating the structure of carbon nanotube devices.

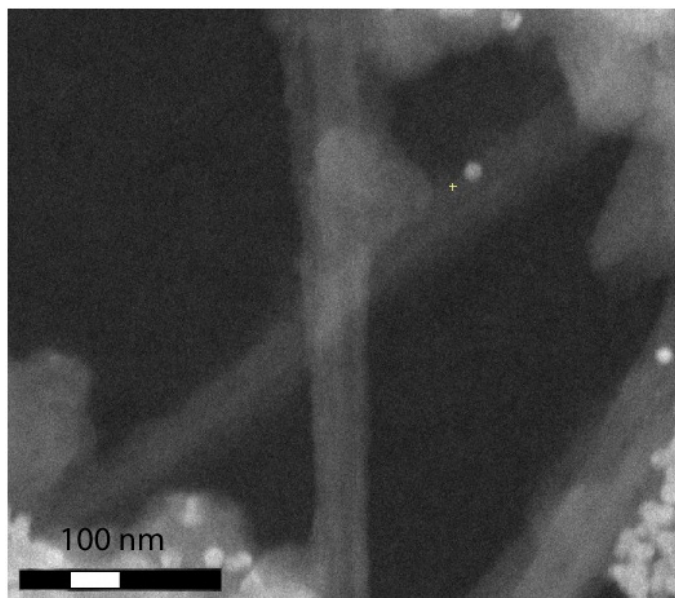


FIG. 11: In this TEM image two carbon nanotubes are projected through one another. The small spheres are 5 nm gold particles used to align successive images in the series. From this image alone it is not possible to determine the separation between the nanotubes

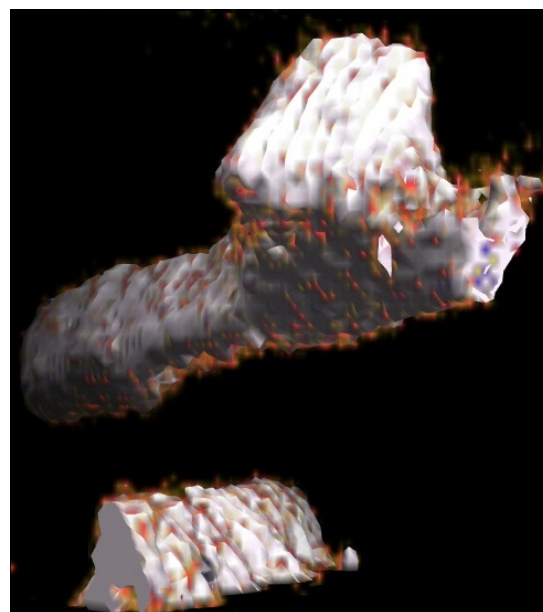
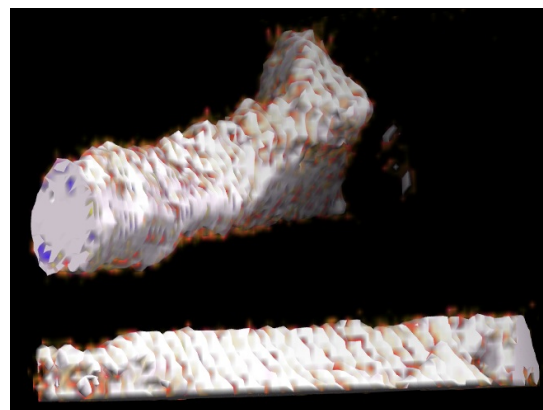
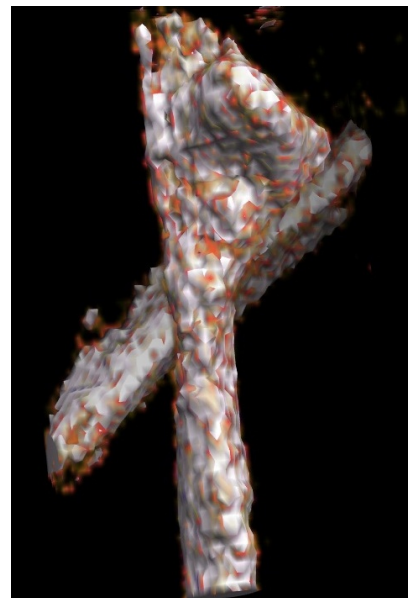


FIG. 12: Several views of a tomographic reconstruction imaged using Chimera reveal 3D details of two carbon nanotubes. The top image is the same view as seen in Fig. 11

XII. SUGGESTIONS FOR FURTHER RESEARCH

I was unable to obtain fully suspended graphene samples of a sufficient size to do tomography this summer. Further research will involve doing tomography on a suspended sheet of graphene in order to observe its characteristic ripples. We will then look at how the ripples are distributed on the sheet. The various amplitudes and wave lengths will be put on a histogram and we will attempt to fit the distribution to a Gaussian or Lorentzian function. Also we will tomographically reconstruct carbon nanotube light bulbs to gain insight on the structural changes that occur when they radiate.

Given the current limit of tomography it is theoretically possible to reconstruct a small carbon nanotube and resolve individual walls. A resolution of $d_z = .33$ nm is possible in reconstructing an object of diameter

$D = 15$ nm using $N = 141$ views. This corresponds to a tilt increment of $\theta = 1^\circ$ and a maximum tilt angle of $\alpha = 70^\circ$. This resolution is right at the edge of what is currently possible given the limitations of our equipment and is the subject of ongoing investigation.

Acknowledgments

I would like to thank Matt Mecklenburg for all his guidance, time and patience this summer. Also thanks to Professor Regan and the rest of his lab for allowing me to join their research team. Thanks to the Hong Zho lab for tomography help and allowing me to use their facilities. Thanks are also due to the NSF for funding this project. Finally I would like to thank Françoise Queval for all her work in making the 2010 UCLA REU program run smoothly.

-
- [1] N.D. Mermin, *Physical Review*, **176**, 250 (1968).
 - [2] A. Fasolino, J.H. Los and M.I. Katsnelson, *Nature Materials* **6**, 858 (2007).
 - [3] J.C. Meyer *et al.*, *Nature* **446**, 60 (2007).
 - [4] A.K. Geim and K.S. Novoselov, *Nature Materials* **6**, 183 (2007).
 - [5] B.W. Smith and D.E. Luzzia, *Journal of Applied Physics* **90**(7), 3509 (2001).
 - [6] A. Zobelli A. Gloter C.P. Ewels G. Seifert and C. Colliex, *Physical Review B* **75** (2007).
 - [7] L. Reimer *Transmission Electron Microscopy* (Springer ,2009)
 - [8] P. Delhaes, *Graphite and Precursors* (CRC Press, 2001).
 - [9] C. Kittel, *Introduction to Solid State Physics* (John Wiley & Sons, Hoboken, 2005).
 - [10] N.W. Ashcroft and N.D Mermin, *Solid State Physics* (Thompson, 1976).
 - [11] P.R. Bevington and D.K. Robinson, *Data Reduction and Error Analysis for the Physical Sciences* (McGraw Hill 2003).
 - [12] R.A. Crowther, D.J DeRosier and A. Klug, *Proc. Roy. Soc. Lond. A.* **317**, 319 (1970).
 - [13] J.C. Russ, *The Image Processing Handbook* (CRC Press, Boca Raton, 2007).
 - [14] R. Guckenburger, *Ultramicroscopy* **9**, 167, (1982).
 - [15] Technical details of these algorithms are not very important for the research presented but it is important to know that the SIRT method creates more accurate reconstructions than the WBP method.
 - [16] P.A. Midgley, M. Weyland, *Ultramicroscopy* **96**, 413 (2003).